Arsenic uptake by natural calcite: An XAS study

ARTICLE *in* GEOCHIMICA ET COSMOCHIMICA ACTA · JUNE 2011

Impact Factor: 4.33 · DOI: 10.1016/j.gca.2011.03.003

8 AUTHORS, INCLUDING:

Marco Benvenuti
University of Florence
72 PUBLICATIONS **554** CITATIONS
SEE PROFILE

Francesco Di Benedetto
University of Florence
81 PUBLICATIONS **677** CITATIONS
SEE PROFILE

Pierfranco Lattanzi
Università degli studi di Cagliari
116 PUBLICATIONS **1,081** CITATIONS
SEE PROFILE

C. Meneghini
Università Degli Studi Roma Tre
170 PUBLICATIONS **1,828** CITATIONS
SEE PROFILE

ISSN 0016-7037
Volume 75, Number 11
June 1, 2011

ELSEVIER

Geochimica et Cosmochimica Acta

JOURNAL OF THE GEOCHEMICAL SOCIETY
AND THE METEORITICAL SOCIETY

Volume 75, Number 11 June 1, 2011

Articles

Continued on outside back cover

Available online at www.sciencedirect.com
ScienceDirect
Geochimica et Cosmochimica Acta 75 (2011) 3011–3023
Geochimica et Cosmochimica Acta
www.elsevier.com/locate/gca

Arsenic uptake by natural calcite: An XAS study

F. Bardelli [a], M. Benvenuti [b], P. Costagliola [b,*], F. Di Benedetto [b,c], P. Lattanzi [d], C. Meneghini [e], M. Romanelli [c], L. Valenzano [f]

[a] Institut des Sciences de la Terre, Université Joseph Fourier, Maison des Géosciences, 1381 rue de la Piscine, 38400 Grenoble, France
[b] Dipartimento di Scienze della Terra, Università di Firenze, via G. La Pira 4, 50121 Firenze, Italy
[c] Dipartimento di Chimica, Università di Firenze, via della Lastruccia 3, 50019 Sesto Fiorentino, Italy
[d] Dipartimento di Scienze della Terra, Università di Cagliari, via Trentino 51, 09127 Cagliari, Italy
[e] Dipartimento di Fisica "E. Amaldi", Università degli Studi Roma Tre, via della Vasca Navale 84, 00146 Roma, Italy
[f] Michigan Technological University, Physics Department, 1400 Townsend Drive Houghton, MI 49931-1295, USA

Received 26 May 2010; accepted in revised form 23 February 2011; available online 6 March 2011

Abstract

As-bearing travertine rocks from Tuscany (Italy), where previous studies suggested the existence of a $CO_3^{2-} \Leftrightarrow AsO_3^{3-}$ substitution in the calcite lattice, were investigated with X-ray Absorption Spectroscopy (XAS) at the As K-edge (11,867 eV). In two of the studied samples, XANES indicates that As is in the 5+ oxidation state only, and EXAFS analysis reveals a local environment typical of arsenate species. For these samples, the lack of detectable second shell signals suggests a poorly ordered environment, possibly corresponding to an adsorption onto oxide and/or silicate phases. On the other hand, in the third sample XANES reveals a mixed As oxidation state (III and V). This sample also presents evident next nearest neighbor coordination shells, attributed to As–Ca and As–As contributions. The occurrence of next neighbor shells is evidence that part of As is incorporated in an ordered lattice. Furthermore, the local structure revealed by EXAFS is compatible with As incorporation in the calcite phase, as further supported by DFT simulations. The observation of next neighbors shells only in the As(III)-rich sample suggests the substitution of the arsenite group in place of the carbonate one ($CO_3^{2-} \Leftrightarrow AsO_3^{3-}$). The conclusion of this work is that uptake of As by calcite is in general less favored than adsorption onto iron oxhydroxides, but could become environmentally important wherever the latter phenomenon is hindered.

1. INTRODUCTION

Arsenic contamination of groundwater and food represents a serious environmental problem in many parts of the world (e.g., Matschullat, 2000; Smedley and Kinniburg, 2002). A wide range of studies have recently been devoted to the mobility of arsenic in natural media, and much attention has been paid to sorption–desorption and coprecipitation reactions between arsenic and mineral surfaces, especially Fe- and Mn-oxyhydroxides (e.g., Lenoble et al., 2002; Sherman and Randall, 2003; Dixit and Hering, 2003; Ouvrard et al., 2005). In particular, adsorption of arsenic by Fe- and Mn-oxyhydroxide surfaces is considered among the most important and widespread mechanisms controlling arsenic mobility. The destabilization of these phases, or the desorption of As oxyanions from their surfaces, is considered one of the pathways to the human food chain (Nriagu, 1994; Tufano et al., 2008 and reference therein). Under some conditions, this mechanism represents a transient immobilization for arsenic.

The possible role of calcite in sequestering As has been considered in a number of studies (Goldberg and Glaubig, 1988; Sadiq, 1997; Cheng et al., 1999; Le Guern et al., 2003; Roman-Ross et al., 2006; Di Benedetto et al., 2006; Alexandratos et al., 2007; Fernández-Martínez et al., 2008;

* Corresponding author. Tel.: +39 55 2757476; fax: +39 55 2757455x284571.
E-mail addresses: pilario.costagliola@unifi.it (P. Costagliola), francesco.dibenedetto@unifi.it (F. Di Benedetto).

0016-7037/$ - see front matter © 2011 Elsevier Ltd. All rights reserved.
doi:10.1016/j.gca.2011.03.003

Sø et al., 2008; Yokoyama et al., 2009). The consequences of As uptake by calcite in natural systems are of considerable relevance because of the ubiquity of this mineral in the Earth's crust and its stability in a variety of geologic environments; therefore, calcite could represent an effective agent for As immobilization.

Most studies are focused on the possibility that calcite may adsorb As-oxyanions onto its surface. In the last four years, however, it was demonstrated that As oxyanions may substitute for the carbonate group in the calcite structure (Di Benedetto et al., 2006; Roman-Ross et al., 2006; Alexandratos et al., 2007). This replacement should be possible in spite of the remarkable size and geometry differences between the carbonate group (C–O distance ~1.3 Å, planar shape) and As oxyanions (As–O ~1.8 Å in arsenite, and ~1.7 Å in arsenate, both of pyramidal shape), because of the known flexibility of the calcite structure (e.g., Tang et al., 2007). There are, however, a number of significant gaps in the knowledge and understanding of the phenomenon. Firstly, most of the studies refer to laboratory conditions, and the extension of their results to natural environments is only inferred. Roman-Ross et al. (2006) indicate that As(III) oxyanions replace CO_3^{2-} groups up to concentrations on the order of 30 mM (~2 g/kg) As, whereas Alexandratos et al. (2007) provide a model in which the incorporation involves As(V)-oxyanions. In a recent study, Sø et al. (2008) cast some doubt on the results by Roman-Ross et al. (2006), concluding that arsenite uptake at the calcite surface can occur only at comparatively high pH and arsenite concentrations. The feasibility of the $CO_3^{2-} \Leftrightarrow AsO_3^{3-}$ replacement mechanism in natural calcite was first inferred by Di Benedetto et al. (2006) in a study of Quaternary travertine deposits in Southern Tuscany (Italy). These authors applied a spectroscopic technique, Electron Spin Echo Envelope Modulation (ESEEM) spectroscopy, whereby the presence of As is detected from its nuclear modulation of the spectrum of the paramagnetic ion Mn(II), which substitutes for Ca in the calcite lattice. The estimated As–Mn distance is comparable with the Ca–C distance in calcite. However, the employed technique does not allow the estimation of the amount of arsenic sequestered by calcite, nor determination of As oxidation state. Thus, an estimate of the actual role played by calcite in natural processes of As-sequestration awaits the full assessment of the process through which As is included in the calcite lattice.

X-ray Absorption Spectroscopy (XAS) is a well established technique for structural investigation (Lee et al., 1981) and chemical speciation (Wilke et al., 2001; Isaure et al., 2002) and, with the development of beamlines able to measure highly diluted elements (down to ppb) at high spatial resolutions, it is gaining increasing importance in the fields of environmental science and geochemistry (Fenter et al., 2002; Alexandratos et al., 2007; Fernández-Martínez et al., 2008; Chakraborty et al., 2010; Aurelio et al., 2010).

In this study, we used XAS to examine samples from the same travertine sequence studied by Di Benedetto et al. (2006), with the aim of investigating the oxidation state, geometry, and local structure of As-oxyanions, and their possible replacement of carbonate groups in the calcite lattice.

2. EXPERIMENTAL

2.1. Background information for natural samples

An anomalous As-rich travertine sequence, located along the valley of the Pecora River (PRV, Southern Tuscany, Italy) was sampled. For a detailed mineralogical and geological description, the reader is referred to Costagliola et al. (2004, 2008, 2010), Di Benedetto et al. (2006), and Benvenuti et al. (2009).

Travertines were formed in a lacustrine environment and make up a sequence having a thickness up to 15–20 m of *carbonatic tufa* of *meteogenic travertine* (*sensu* Pentecost, 1995). In the paleolake, where travertine accumulated, there was a concomitant, intermittent deposition of siliciclastic sediments. As a consequence, travertines are composed mostly of calcite in micro-crystals forming a vacuolar texture (Fig. 1), and by variable amounts of other minerals (mainly silicates), including Fe-oxyhydroxides, conferring to the bulk rock a brownish-yellow color. Non-carbonate minerals (essentially quartz, mica, clay minerals, and Mn and Fe-oxyhydroxides) may be found as discrete thin layers (Fig. 1). In addition to Ca, travertine cation composition includes minor amounts of Si, Al, Mg and Fe (Di Benedetto et al., 2006). Bulk As-contents range between 127 and 257 mg/kg. Application of an *ad hoc* implemented sequential extraction procedure demonstrated that a significant part (tens to hundreds of mg/kg) of this element is specifically linked to the calcite fraction (Costagliola et al., 2007). Arsenic may have been introduced in the paleolake along with the siliciclastic sediments (Di Benedetto et al., 2006; Costagliola et al., 2008, 2010; Benvenuti et al., 2009).

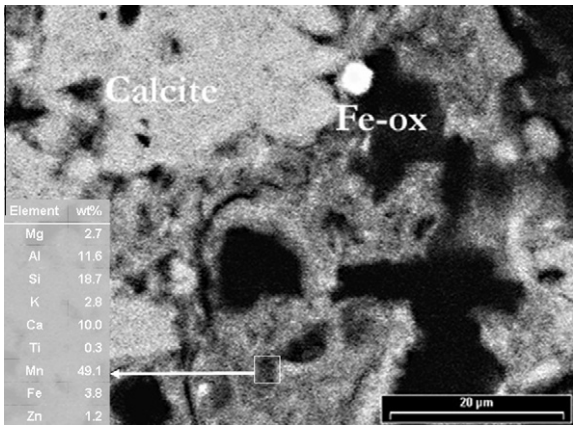

Fig. 1. SEM image (backscattered electrons) of a travertine sample. It is evident the vacuolar structure of the rock (dark holes). Calcite is in medium grey, whereas small crystals of Fe-oxyhydroxides are present at the top (white). The medium grey-dark area at the bottom is presumably composed by a mixture of Mn(Fe)-oxyhydroxides, calcite and silicates. The semi-quantitative EDS analysis of one of the latter regions (white rectangle) is provided in the table.

In this study three different aliquots (F1b, F1bM and F1bNM) of a travertine sample (F1b, studied by Di Benedetto et al., 2006) were examined. This sample was selected since it had the highest As-content of the sequence (257 mg/kg; see Table 1 of Di Benedetto et al., 2006), and was already studied by these authors via EPR-ESE spectroscopy. The three different aliquots are the result of a separation of the mineral phases carried out by means of a magnetic isodynamic Frantz separator (F1b: raw sample; F1bM and F1bNM: "magnetic" and "non-magnetic" fractions of F1b, respectively). We expected a significant separation of magnetic Fe-oxyhydroxides from diamagnetic minerals (including calcite); however, even if qualitative X-ray Fluorescence (XRF) spectra acquired at 12 keV on the Italian beamline at the European synchrotron (ESRF), confirmed Fe to be enriched in the magnetic F1bM fraction (Fig. 2), X-ray Diffraction (XRD) patterns of the bulk sample and of the two fractions did not show differences. Nevertheless, it has to be noted that detection limit of XRD technique (3–5 wt.%) and poor crystallinity of the unique

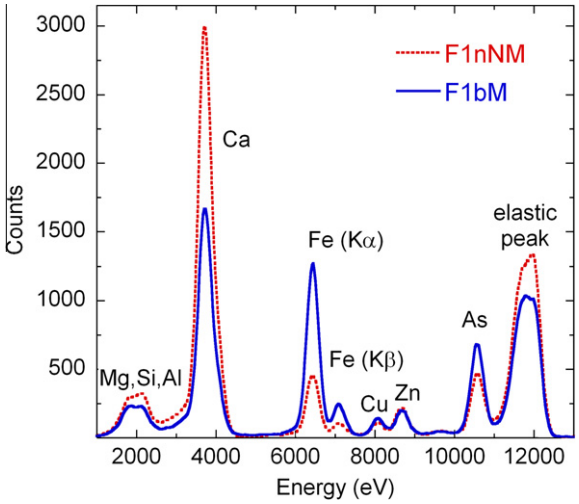

Fig. 2. Qualitative fluorescence spectrum of the F1bM and F1bNM samples: Fe-content is observed to increase in the magnetic fraction F1bM.

Table 1
Coordination numbers (CN), bond distances (R) and Debye–Waller factors (σ^2) of all reference compounds and travertine samples. Coordination numbers of reference compounds were kept fixed to their crystallographic values.

As(III) samples + F1bNM	Path	CN	R (Å)	σ^2 (Å^2) × 10^3	S_0^2
Na-arsenite	As–O(1)	1	1.69(3)	1.9(9)[a]	1.0(2)
$NaAsO_2$	As–O(2)	2	1.80(2)	5.5(9)	
As(III)	As–As	2	3.22(2)		
Arsenic (III) oxide	As–O(1)	3	1.80(1)	1.7(9)	0.8(1)
As_2O_3	As–O(2)	3	3.00(5)	4.7(9)	
As(III)	As–As(1)	3	3.25(1)	1.1(9)	
	As–As(2)	6	3.93(4)	12(1)	
F1bNM	As–O	3.3(5)	1.74(1)	6(1)	1[b]
As(V)–As(III)	As–Ca(1)	1.5(7)	3.07(1)	4(2)[a]	
	As–Ca(2)	2.1(8)	3.36(1)		
	As–As	4(2)	3.93(2)	12(5)	
As(V) samples	**Path**	**CN**	**R (Å)**	**σ^2 (Å^2) × 10^3**	**S_0^2**
F1B	As–O	4	1.68(2)	2	1.0(1)
As(V)				.4(2)	
F1BM	As–O	4	1.68(3)	2.4(9)	1.0(2)
As(V)					
Ferrihydrite	As–O	4	1.69(2)	1.3(2)	1.0(1)
$Fe(OH)_3$	As–As	1.1(5)	3.34(3)	2.6(6)[a]	
As(V)	As–Fe	1.7(9)	3.26(2)		
Scorodite	As–O	4	1.69(1)	1.1(8)	0.9(1)
$Fe(AsO_4)(H_2O)_2$	As–Fe	2	3.33(3)	3.8(9)	
As(V)	As–Fe	2	3.51(6)	8.5(9)	
Na-arsenate	As–O(1)	4	1.69(1)	0.8(1)	0.8(1)
$NaH_2(AsO_4)(H_2O)$	As–O(2)	1	3.21(4)	1.0(1)	
As(V)	As–Na(1)	2	3.69(4)	4.9(6)	
	As–Na(2)	4	3.93(4)	5.0(7)	
Arsenic (V) oxide	As–O(1)	2	1.67(3)	2.7(2)[a]	0.9(1)
As_2O_5	As–O(2)	3	1.80(4)		
As(V)	As–As(1)	2	3.10(3)	7.2(6)	
	As–As(2)	2	3.23(4)	7.9(6)	
Ca-arsenate	As–O	4	1.68(1)	2.0(4)	1.0(1)
$Ca_3(AsO_4)_2$	As–Ca(1)	1	3.27(6)	6(1)	
As(V)	As–Ca(2)	3	3.56(8)	9(1)	
	As–Ca(3)	3	3.71(6)	9(2)	

[a] The same Debye–Waller factor parameter was used for these paths.
[b] S_0^2 was arbitrarily fixed to 1 to avoid strong correlation with CN. Numbers within parenthesis represent the uncertainty on the last digit.

magnetically active phases of the investigated sample (i.e., Fe-, Mn-oxy-hydroxides) could have prevented their identification.

2.2. SEM-EDS

Morphological, mineralogical and semi-quantitative chemical microanalyses were performed on graphite-coated polished sections using a Philips SEM515 Scanning Electron Microscope (SEM) equipped with an AnalySis-ADDA image grabber and an Edax Falcon X-ray Energy Dispersive Microanalytical System.

2.3. DFT simulations

Numerical simulations of the arsenite inclusion in the calcite structure were carried out using periodic Density Functional Theory (DFT) calculations employing the hybrid B3LYP functional (Becke, 1993; Lee et al. 1988). All calculations were performed with the CRYSTAL06 code (Dovesi et al., 2006).

The CRYSTAL package performs *ab initio* calculations of the ground state energy, energy gradient, electronic wave function, and properties of periodic systems at both Hartree–Fock and Kohn–Sham level of theory. The fundamental approximation made is the expansion of the single particle wave functions (crystalline orbitals) as a linear combination of Bloch functions defined in terms of local functions (atomic orbitals). The local functions are, in turn, linear combinations of Gaussian type functions whose exponents and coefficients are defined by input. Functions of symmetry s, p, d and f can be adopted, and also available are sp shells.

For calcium, oxygen, and carbon atoms, all-electron Gaussian-type basis sets were used, as reported in Valenzano et al. (2006); for arsenic, the Durand and Barthelat effective core pseudo-potential was used, as reported in Causà et al. (1991). For numerical integration of the exchange–correlation term, a (75,974)p pruned grid was adopted, and the condition for the SCF convergence was set to 10^{-7} Hartrees during geometry optimization. A full relaxation of the structures (both lattice parameters and atomic positions) was performed. For geometry optimization, the default convergence criteria were used. In particular, an estimated model Hessian is adopted in the program and the matrix is stored at each optimization step, allowing the possibility, for example, to restart the calculation at another level of theory. Different Hessian updating schemes are available for minimization; in the reported calculations, the so called BFGS Hessian update scheme by Broyden–Fletcher–Goldfarb–Shanno (Broyden, 1970a,b; Fletcher, 1970; Goldfarb, 1970; Shanno, 1970) was employed. This is the default method used in CRYSTAL to update the Hessian matrix.

The convergence criteria on the RMS of the gradient and the displacement were set to 0.0003 and 0.0012, respectively. Nevertheless, a more sophisticated and accurate technique to control the step size was adopted: the *trust radius region scheme* that limits the step length of the displacement at each cycle, according to the quadratic form of the surface in the actual region. The default maximum value for minimization is 0.5. At each optimization cycle, the step is computed by means of a Newton-like scheme, while the length is determined by linear minimization along an extrapolated quadratic polynomial.

Since both total energy and gradients are affected by the integrals classification (truncation of infinite Coulomb and exchange series), a single-point energy calculation needs always to be run with the final structure, and integrals have to be re-classified according to the new final geometry to calculate correct total energy and gradients. If during this final run procedure the convergence test on the forces is not satisfied, optimization is restarted, keeping the integrals classification based on the new geometry. For this reason, the FINALRUN option has to be used. Among the different levels of choice, we chose the tighter, which computes single-point energy and gradient followed by a new optimization process starting from the final geometry of the previous one (used to classify the integrals); if the convergence test is not satisfied the procedure iterates until full stable optimization is reached.

The experimental unit cell of pure calcite structure (Markgraf and Reeder, 1985) was used as starting point for the model. A single unit cell was used for the calculations where one of the CO_3^{2-} ions, placed in the bulk of the cell, was replaced with an $HAsO_3^{2-}$ unit to avoid any surface effect in the volume expansion. Despite the apparent simplicity of the model, we believe that this approach is sufficient to provide a comparison with the local structure experimentally obtained by means of the XAS technique. Nevertheless, we want to stress here that the model used is not suitable for a comparison with the long range structure. Such a comparison would have been possible only using a large supercell, in order to let the structure around the inserted As defect relax.

The presence of the hydrogen atom was necessary to ensure the charge neutrality. The geometrical optimizations were made at zero temperature and removing symmetry constraints (space group: P1).

2.4. XAS setup

X-ray Absorption Spectroscopy (XAS) measurements at the As K-edge (11,867 eV) were performed at the GILDA (BM-08) beamline (Pascarelli et al., 1996) at the European Synchrotron Radiation Facility (ESRF, Grenoble – France). The main beamline optical features include a fixed exit monochromator with a pair of Si [3 1 1] crystals, and a pair of Pd coated mirrors for efficient harmonic rejection and (vertical) focusing of the X-ray beam. A dynamic sagittal (horizontal) focusing of the X-ray beam is realized by bending the second monochromator crystal. This provides a sub-millimetric (~250 μm horizontal, 150 μm vertical) X-ray spot on the sample, with a photon flux at 12 keV of about 10^9 ph s^{-1}. Considering the monochromator crystals and the vertical aperture of slits at the source (1 mm), the energy resolution was calculated to be about 0.5 eV at the As K edge. The energy sampling interval in the higher resolution near edge region (11,840–11,920 eV) was 0.2 eV. In order to reduce the dumping of the signal due

to the thermal contribution and to prevent possible beam-induced redox reactions, all samples were measured at liquid nitrogen temperature (77 K).

Reference compounds included: pure synthetic arsenic(III) and arsenic(V) oxides, As_2O_3 and As_2O_5 (Alfa Aesar), calcium and sodium arsenate, $Ca_3(AsO_4)_2$ and $Na_2HAsO_4{\cdot}7H_2O$ (Alfa Aesar), sodium arsenite, $(NaAsO_2)_x$, and natural scorodite, $FeAsO_4{\cdot}2H_2O$, kindly provided by the Museo di Storia Naturale (Mineralogy Section) of the Università di Firenze. In addition, an As-bearing Fe-oxyhydroxide was synthesised in the laboratory by precipitation from a As-, Fe-acidic solution through pH increase (Jia et al., 2007). Phase and crystallinity check of natural scorodite and synthetic Fe-oxyhydroxide was performed by XRD. Both samples were found monophasic, and the Fe-oxyhydroxide revealed the characteristic two-line structure (Schwertmann et al., 2004).

All reference samples were prepared for XAS measurements as follows: we calculated the amount suitable to reach an edge step ($\Delta\mu t$) close to 1 while keeping the total absorption (μt) in the range 1–2.5; this amount was mixed and homogenized with cellulose in an agate mortar. The mixture was then pressed at 10 bars into 25 mm diameter pellets that were then mounted on a copper sample holder, placed in a vacuum chamber (10^{-5} mbars), and cooled down to liquid nitrogen temperature (77 K).

All reference compounds spectra were collected in transmission geometry, i.e., measuring the intensity of the X-ray beam upstream (I_0) and downstream (I_t) of the sample by means of ionization chambers filled with suitable gas and pressure (20% absorption in the upstream chamber, 80% in the downstream one). A third ionization chamber was placed after a second experimental chamber containing an As_2O_3 standard which spectrum was acquired simultaneously with each sample spectra and used for accurate energy calibration. Depending on the quality of the spectra, a minimum of two scans were collected, interpolated and averaged to increase the signal-to-noise ratio.

Powdered travertine samples were either pressed in pellets, or diluted in ethanol and deposited onto microporous membranes. Because of the low arsenic content (~200 mg/kg), travertine samples were measured in fluorescence mode by means of a 13-elements solid state (high purity Germanium) detector (ORTEC). A minimum of three spectra were collected for each travertine sample, and averaged to improve the statistics of the data. Higher integration times (up to 30s) per energy point were preferred to a larger number of scans, because of the long dead-time of the acquisition system and the limited beamtime available.

Standard procedures (Rehr and Albers, 2000) were followed to extract the structural EXAFS (Extended X-ray Absorption Fine Structure) signal ($k \cdot \chi(k)$): pre-edge background removal, spline modeling of bare atomic background, edge step normalization using a far above the edge region, and energy calibration.

Model atomic clusters centered on the absorber atom were obtained by ATOMS (Ravel, 2001) using crystallographic structures reported in the literature (Menary, 1958; Gopal and Calvo, 1971; Ferraris et al., 1974; Kitahama et al., 1975; Pertlik, 1978; Jansen, 1979; Jansen et al., 2002) as input. Theoretical amplitude and phase functions were generated using the FEFF8 code (Ankudinov et al., 1998). The FITEXA code (Monesi et al., 2005), used for refinement of the EXAFS signal, exploits the MINUIT routines of CERN libraries (James and Winkler, 2004) for least square minimization. Errors on structural parameters were calculated using the MINOS subroutine from the MINUIT package, and takes into account the correlation between parameters.

The number of floating parameters during minimization never exceeded 12, which is lower than the maximum number of independent points ($N_{ind} = (2 \cdot \Delta k \cdot \Delta R/\pi + 1 = 17$, Δk and ΔR being the k (reciprocal space) and R (direct space) ranges of useful data). For a maximum useful extension of the spectra of $k_{max} = 14$ Å^{-1}, the theoretical spatial resolution of our data is 0.02 Å ($\delta R \sim \pi/(2 \cdot k_{max})$). Actual resolution is lower due to the noise contribution to the spectra, and was estimated to be about 0.05 Å.

For XANES (X-ray Absoption Near Edge Structure) semi-quantitative analysis, all spectra were normalized to a region far from the edge step (>200 eV), and the energy scale was carefully calibrated using the reference absorption spectra from As_2O_3 simultaneously acquired at each scan.

Structural information (number and type of neighboring atoms, bond distances and structural disorder) around the absorber atom were extracted from the analysis of the extended region of the absorption spectra (Extended X-ray Absorption Fine Structure: EXAFS).

Data refinements were performed in the back-transformed space, applying the standard XAFS formula (Rehr and Albers, 2000). For direct comparison all the spectra (travertine and references samples) were treated and fitted using the same parameters: Fourier transform (FT) range 1–14 Å^{-1} (13.3 Å for F1bNM sample) and weight 3, back-Fourier transform (BFT) range 1–3.5 Å (uncorrected for phase shift). The fitting range was 4–14 Å^{-1} (in the back-transformed space) and the fitting weight 3. Such a large starting point (4 Å^{-1}) for minimizations was chosen to avoid strong near edge multiple scattering effects, and because theoretical amplitude and back-scattering functions calculated by *ab initio* multiple scattering based codes, such as FEFF, are less accurate in the low k-region.

For all samples, only single-scattering paths were found relevant to fit the spectra. Experimental energy shift (DE) was optimized through a first shell analysis and kept fixed during final full spectra refinements. Coordination numbers (CN) of all reference compounds were kept fixed to their crystallographic values in order to avoid correlation with the amplitude reduction (S_0^2) and Debye–Waller (σ^2) factors. More details on the strategy followed for refinements of travertine samples are given in the EXAFS section.

3. RESULTS

3.1. XANES

XANES absorption spectra of all measured samples (reference compounds and travertine samples) are reported in the left panel of Fig. 3. Edge crests (i.e., the main peak after the absorption edge) and absorption edges energies

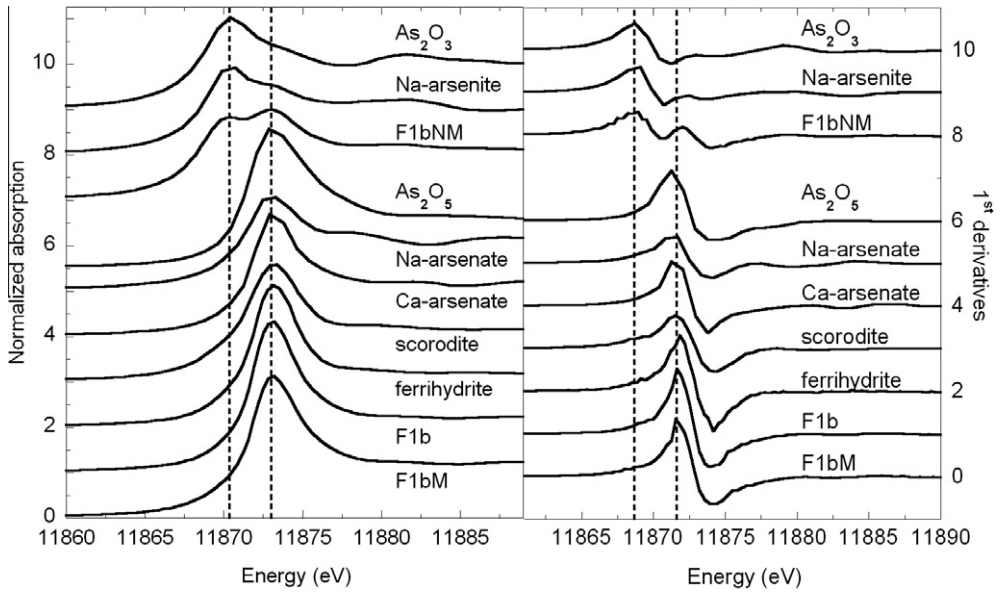

Fig. 3. Calibrated and normalized XANES spectra of travertine samples (F1b, F1bM and F1bNM) and of all measured reference compounds (left panel). Note the similarity of the position of the main edge crest of F1b and F1bM and the all the other As(V) compounds (11,873 eV), while F1bNM have a double edge crest which positions match As(V) and As(III) edge crests (11,870 and 11,873 eV). Right panel: first derivatives of the absorption spectra of all spectra reported in the left panel. The peaks in the derivatives indicate the position of the main inflection point, which, by convention, is considered to be the absorption edge energy (E_0). It can be seen that all As(III) compounds have an absorption edge at 11,868.6 eV, and all As(V) compounds at 11,871.6 eV (1.6 and 5.6 eV above the elemental As edge, respectively). Again F1bNM show two peaks at energies corresponding to As(III), As(V) edges (11,868.6 and 11,872 eV). Vertical dashed lines are a guide to the eye to highline As(V) and As(III) edge crests. Spectra are vertically shifted for ease of view.

(position of the first peak of the derivative of the absorption spectra, Fig. 3, right panel) are separated in two groups: As(V) reference compounds and F1b, F1bM travertine samples (average edge crest, 11,873 eV, absorption edge 11,871 eV), and As(III) reference compounds (average edge crest, 11,870 eV, absorption edge 11,869 eV). These values are in agreement with the literature (Jönsson and Sherman, 2008), reporting energies about 1.5 and 5.5 eV above the elemental As K-edge (11,867 eV) for As(III) and As(V) species, respectively.

A double edge crest occurs in F1bNM's spectrum, at energies corresponding to those of As(III) and As(V) reference compounds (Fig. 3, left panel); this appears in two peaks in the first derivative at energies corresponding to As(III) and As(V) adsorption edges (Fig. 3, right panel). This is clear evidence of a mixed As oxidation state (III/V) in F1bNM.

The XANES features of F1b and F1bM travertine samples are similar to those of both scorodite and arsenate spectra, showing a smooth trend after the edge crest, whereas Ca- and Na-arsenates have slightly more structured spectra (Fig. 3), representing poorer matches to F1b and F1bM.

F1bNM more structured spectrum originates from the superposition of signals arising from As(III) and As(V) local environments. This is supported by the fact that F1bNM spectrum can be reproduced using a normalized linear combination of As_2O_5 and As_2O_3 spectra $\mu_{sample} = x \cdot \mu(As_2O_5) + (1 - x) \cdot \mu(As_2O_3)$. The weighting factor of the linear combination (x) was optimized using the XPSFIT code (Bardelli et al., 2009) and indicates a ratio of As(III) to As(V) of roughly 3:1 (Fig. 4). It is worth noting that this procedure was only used to estimate the As(III)/As(V) ratio in F1bNM and does not imply that F1bNM is a mixture of the arsenic oxides.

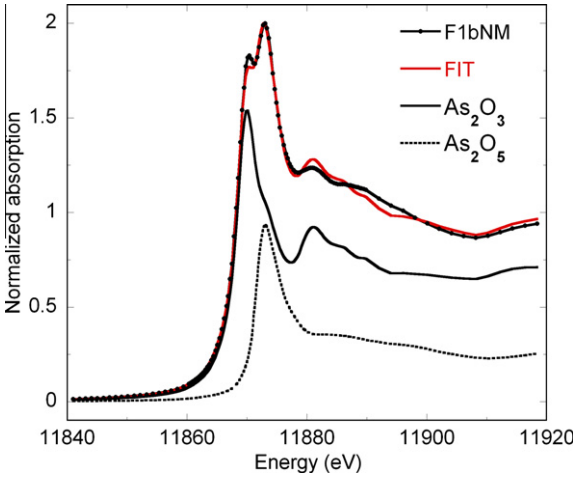

Fig. 4. Linear square fit of F1bNM (solid line) using a linear combination of the As(V)- and As(III)-oxide spectra. The experimental F1bNM spectrum is reported in points + line style together with the relative contributions of As(V)-(dashed line) and As(III)-oxides (solid line).

3.2. EXAFS

Back-Fourier transformed (BFT) EXAFS oscillations of As(III) standards, plus F1bNM travertine sample, are reported in the left panel of Fig. 5 (upper panel), together with the corresponding fit curves, while BFT and fit curves of As(V) standards plus F1b and F1bM travertine samples are shown in the lower left panel of the same figure. Fourier transform moduli (|FT|) of the EXAFS oscillations of the standards and samples reported in the left panels are shown in the right panels (As(III) plus F1bNM, upper panel; As(V) plus F1b and F1bM, lower panel) together with the corresponding fit curves. |FT|s represent a radial distribution function of distances centered on the absorber atom. Each peak corresponds to an average length (provided a correction for a phase function) arising from a single scattering path or, due to the limited resolution, is the convolution of peaks corresponding to different paths. The first peak (around 1.4 Å, uncorrected for phase shift) is always related to the first oxygen coordination shell (As–O paths), while peaks at higher R values correspond to As–Fe, As–Ca, As–Na, and/or As–As contributions, depending on the compound considered.

In the following we describe the refined local structure around the arsenic atom of F1b and F1bM together, and consider the F1bNM sample in a separate paragraph.

3.2.1. F1b–F1bM

As can be seen from Fig. 5 (lower left panel), F1b and F1bM have an almost single-frequency oscillation reflecting in a single well defined peak in the real (R) space (Fig. 5, lower right panel). This means that virtually no contributions from coordination shells higher than the first are detectable, suggesting a poor crystalline structure of adsorbate. Structural refinements reveal that F1b and F1bM have nearly identical local structure: four As–O bonds at

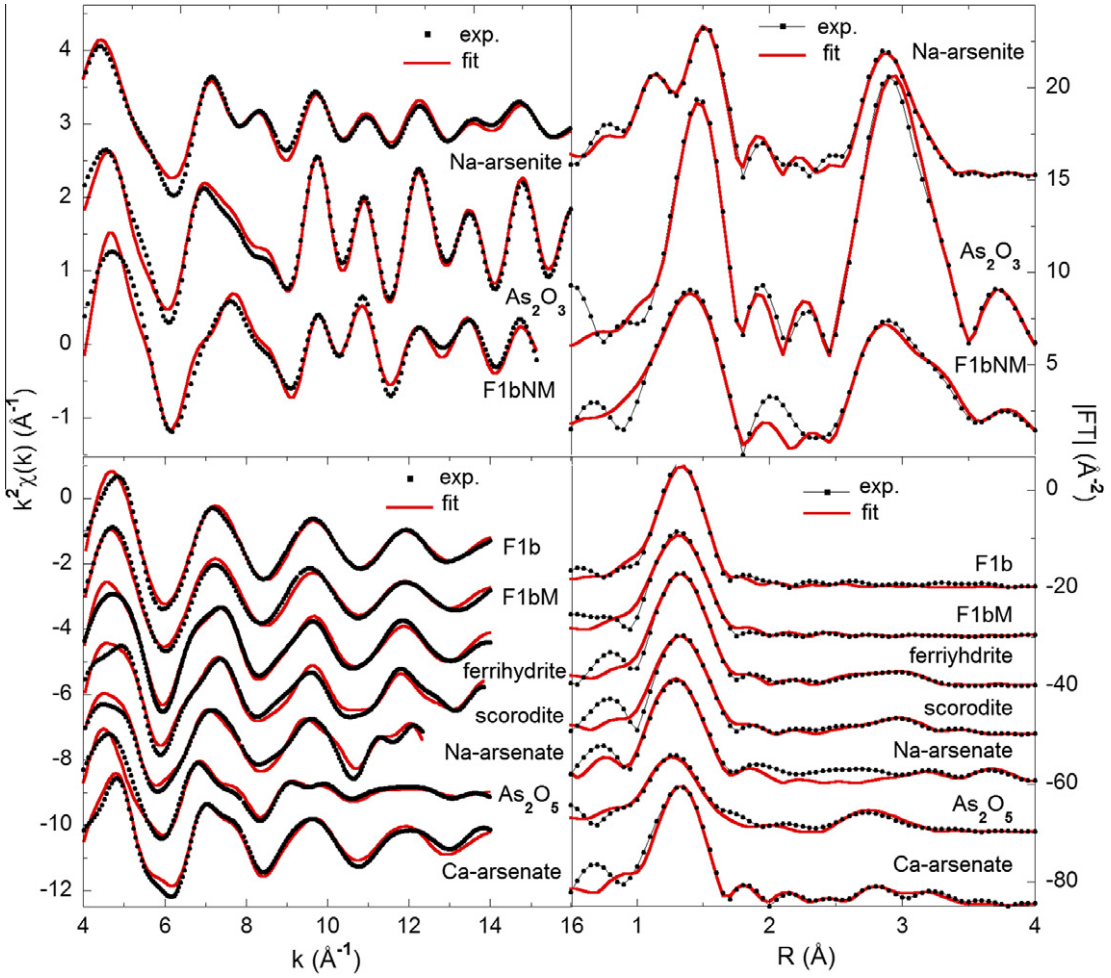

Fig. 5. Left panels: back-transformed (1 ÷ 3.5 Å) EXAFS signals (points) of the As(III) plus F1bNM (upper panels), and As(V) standards plus F1bNM (lower panels), and corresponding fit curves (solid grey line). Fits were performed in the k-space (4 ÷ 14 $Å^{-1}$). Right panel: FT (4 ÷ 14 $Å^{-1}$) of the signals and fit curves reported in the right panel (experimental, points + line; fit curves, solid gray line). Values in the real space (R) are not corrected for the phase shift. Note the difference between less structured spectra of As(V) compounds, which reflects in low or negligible peaks at $R > 2$ Å in the FTs (contributions from shells higher than the first), and more structured spectra of As(III) compounds and F1bNM, which, conversely, have relevant higher shell contributions. Spectra are vertically shifted for ease of view. (For interpretation of the references to colour in this figure legend, the reader is referred to the web version of this article.)

a distance of about 1.68 Å. Coordination numbers were set to four in final refinements to avoid the strong correlation with the EXAFS amplitude reduction factor S_0^2. This assumption is supported by XANES results, revealing As in the 5+ oxidation state (arsenate groups, AsO_4^{-3}, have tetrahedral structure, Fig. 6c). Further support to this model comes from the facts that:

(1) F1b and F1bM XANES spectra are similar to scorodite, ferrihydrite, Na- and Ca-arsenate reference compounds spectra, where As is present as arsenate (see Fig. 3);
(2) low values of the Debye–Waller factors ($\sim 2 \cdot 10^{-3}$ Å^2), suggest equal As–O bond distances and a well ordered first coordination shell, as occurring for the arsenate group (see Table 1);
(3) fixing the coordination number to 4, a stable minimum for the amplitude reduction factor (S_0^2) is found in the range of physically meaningful values ($0.7 \div 1.0$), close to that of all other As(V) reference compounds (see Table 1).

3.2.2. F1bNM

Since the EXAFS signal in F1bNM originates from an admixture of As sites (arsenite and arsenate), having different local structures, it was not possible to fix CNs to theoretical values as done for F1b and F1bM. The lack of a reliable model to fit such an unknown structure led us to arbitrarily setting the amplitude reduction factor (S_0^2) to 1, to avoid the strong (anti)correlation with CNs. Considering that S_0^2 lies in the range 0.8–1.0 for all structures refined in this work (Table 1), we estimated that this assumption introduces an error on the refined CN not larger than ~20%, which is the usual error attributed to CNs in EXAFS. Conversely, there was no way to avoid correlation between the Debye–Waller factors (σ^2) and CNs, a common problem in EXAFS refinements (Lee et al., 1981). To reduce the correlation, the same σ^2 parameters were used for the split As–Ca distances. Furthermore, correlations between parameters are taken into account by the minimization routine increasing the error bars according to the correlation matrix.

Refined structural parameters of F1bNM reveal a first oxygen coordination shell with CN lying between 3 and 4

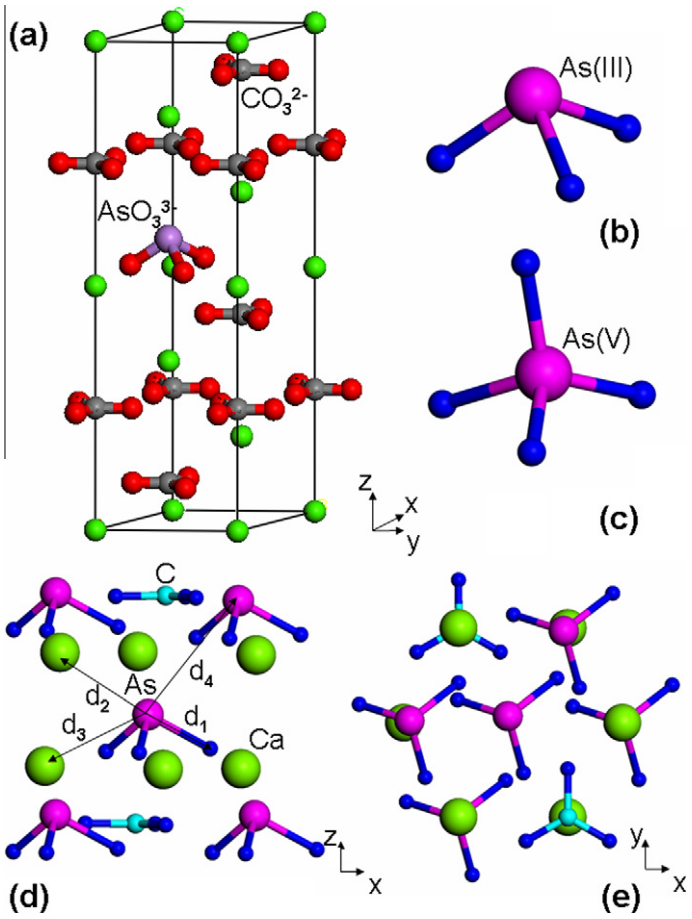

Fig. 6. (a) Representation of the incorporation of an arsenite unit $HAsO_3^{2-}$ in the calcite unit cell. Simulation leads to As atoms displaced out of the arsenite oxygen's plane (along the *c*-axis) while CO_3^{2-} groups remain planar. (b) Molecular geometry of arsenite (AsO_3^{3-}) and (c) arsenate (AsO_4^{3-}) oxyanions in solution (Ramírez-Solís et al., 2004). Local structure around the As(III) atom as resulting from EXAFS refinements projected along the *y* direction (d) and along the *z* direction (e); the arrows labeled d_1, d_2, d_3 and d_4 correspond to the As–O, As–Ca1, As–Ca2, and As–As distances, respectively.

(3.3), and an As–O bond length of 1.74 Å (Table 1). The quite large Debye–Waller value ($\sim 6\times10^{-3}$ Å^2) suggests that this shell is a convolution of As–O sub-shells split at different distances. This is consistent with the two different local environments corresponding to the two As oxidation states suggested by XANES analysis.

In contrast to F1b and F1bM, the mixed oxidation state sample (F1bNM) spectrum has an intense signal from coordination shells higher than the first. According to the bulk chemical analyses (Di Benedetto et al. 2006), which detected Ca, Al, Si, Mg, As and Fe as major elements present in these same samples, different As-backscatterer couples (As–Fe, As–(Si/Al/Mg), As–Ca, and As–As) were used in different combinations to fit higher shell contributions. Mg, Al and Si backscatterers, which are hardly distinguishable by EXAFS, were ruled out after first trials. The most stable and reliable configuration resulted the one with a split As–Ca coordination shell ($R_{\mathrm{As–Ca(1)}} = 3.07$, CN = 1.5, and CN = 2.1, $R_{\mathrm{As–Ca(2)}} = 3.36$ Å), and a longer contribution from an As–As coordination at $R_{\mathrm{As–As}} =$ 3.93 Å (CN = 4), Table 1. A sketch of the local environment of As refined by EXAFS analysis is reported in Fig. 6d and e.

3.3. DFT results

DFT simulations on the calcite unit cell with arsenite replacing carbonate reveal a distorted AsO_3 pyramid with three different As–O distances (Table 2). The As–O1 bond (1.845 Å) is considerably longer than the As–O2 and As–O3 bonds (1.738 and 1.733 Å, respectively). In average the As–O distance is about 1.772 Å, which is longer than the value obtained by EXAFS (about 1.74 Å). Second shell features reveal two different As–Ca distances at 3.042 and 3.316 Å, which are very close to the same distances measured by EXAFS (3.07 ± 0.01 and 3.36 ± 0.01), (Table 1).

The calcite cell parameters calculated by DFT differ from those of the pure calcite, the largest difference being for the length of *c*: 18.239 Å (DFT) versus 17.061 Å (Markgraf and Reeder, 1985). Within the limits of validity of the chosen model, this large difference suggests that incorporation of the pyramidal AsO3 group in place of the triangular CO_3 has a strong effect, especially along the c axis.

4. DISCUSSION

The complete mineral assemblage of the travertine sequence, to which the F1b sample belongs, was studied in detail by Di Benedetto et al. (2006), by complementary analyses including optical microscopy, X-ray diffraction, and SEM-EDS. Beside calcite and variable amounts of quartz, these authors found traces of phyllosilicates, Ca-sulphates, iron-hydroxides, and Ti-oxides. SEM-EDS semi-quantitative analyses pointed out the presence of small iron-oxide fragments with high arsenic contents (up to about 6% by weight). The chemical composition of travertine (major CaO, with variable amounts of SiO_2 and Al_2O_3; Di Benedetto et al., 2006) is consistent with this mineral assemblage. Travertine is rather heterogeneous at the scale of the single outcrop. The large XAS spectral difference between F1b–F1bM, and F1bNM, sub-samples of the same bulk sample, proves this high heterogeneity also at the scale of the single sample.

Samples dominated by As(V) (F1b and F1bM) have a single oxygen first coordination shell, with four almost equivalent As–O bonds at 1.68 Å. Next neighbor features, if present, are negligibly weak. This finding suggests that As, when occurring as arsenate, is not incorporated in any crystalline structure. In particular, the similarity of F1b and F1bM spectra to that of As in ferrihydrite suggests that As(V) could be adsorbed on the surface of poorly crystalline iron-oxyhydroxides, which are well known as strong adsorbers for As(V) oxyanions (Saalfield and Bostick, 2009, and reference therein). Refined structural parameters of F1b and F1bM, in particular the observed low Debye–Waller factor, are evidence for equally compensated charge, suggesting the absorption of protonated As oxyanions rather than $(AsO_4)^{3-}$ (Sherman and Randall, 2003).

In the case of F1bNM sample, the first oxygen shell can be interpreted as a convolution of As–O sub-shells deriving from different local environments for As(V) and As(III). The first shell CN (3.3) is in agreement with the value arising from the average of arsenite and arsenate CNs weighted for the As(III)/As(V) ratio (3:1) determined by linear square fitting of XANES spectra discussed above. The value for the As–O bond length (1.74 Å) is also in accordance with an admixture of different As local structures, being intermediate (if weighted for the arsenite/arsenate 3:1 ratio)

Table 2
Comparison between calculated (DFT), experimental (EXAFS), and crystallographic (ICSD) structural parameters (atomic distances and lattice cell parameters). EXAFS values refer to the F1bNM sample, DFT values to a calcite cell with a single $HAsO_3^{2-}$ unit in place of a CO_3^{2-} one (see text), and crystallographic values refer to the pure calcite cell (Markgraf and Reeder, 1985). The numbers within parenthesis represent the uncertainty on the last digit.

Atomic distances (Å)				Lattice parameters (Å)	
Path	DFT		EXAFS	Calcite cell + $HAsO_3^{2-}$ (DFT)	Crystallographic values (ICSD)
As–O1	1.845	}1.772			
As–O2	1.738		1.74(1)	$a = 4.975$	$a = 4.988(1)$
As–O3	1.733			$b = 5.027$	$b = 4.988(1)$
As–Ca1	3.042		3.07(1)	$c = 18.239$	$c = 17.061(1)$
As–Ca2	3.316		3.36(1)		
C–O1	1.287		–	$\alpha = 87.3°$	$\alpha = 90°$
C–O2	1.288		–	$\beta = 90.0°$	$\beta = 90°$
C–O3	1.286		–	$\gamma = 118.9°$	$\gamma = 120°$

between the As–O distance in the arsenate group (1.68 Å in aqueous solution, Ramírez-Solís et al., 2004; Fig. 6c) and the average value obtained from simulations on the arsenite group substituted in the calcite lattice (1.77 Å, see Table 2).

The occurrence of higher shell contributions in F1bNM suggests that As is here hosted in a more ordered environment with respect to F1b and F1bM samples. It is interesting to note that in F1b and F1bM, characterized by negligible contributions from next neighbor coordination shells, arsenic occurs as As(V) only. Conversely in F1bNM, where arsenic is mainly As(III), next neighbor contributions are more intense and evident (peak in the range 2.5–3.5 Å in the Fourier transform). This fact would suggest that the structural contributions due to the next neighbor coordination shells mainly originate from the As(III) species. The total coordination number of the As–Ca shells, being the sum of coordination numbers of As–Ca sub-shells at 3.07 and 3.36 Å, is CN ~4(1). This value is lower than that expected for As fully substituting for C in the calcite lattice (CN = 6). However, it must be stressed here that only a fraction of As is incorporated into the calcite lattice, i.e., As(III), while As(V), which is probably adsorbed on host structures (Fe/Mn-oxyhydroxides or calcite itself), has negligible second shell contributions (as in F1b and F1bM). Since the amplitude of the EXAFS signal is normalized to the total As amount in the sample, the apparent coordination numbers of the two As species are weighted by the As(III) and As(V) fractions. Therefore, since the As(III)/As(V) ratio is close to 3:1, the fraction of As(III) is about 3/4 and the expected As–Ca CN is $6 \cdot 3/4 = 4.5$, which is higher but consistent with our finding within error. Concerning the As–As contribution around 3.9 Å, its CN is expected to depend on the dilution level and distribution of As ions in the host structure: random distribution and low concentrations of As leads to a reduction of the As–As CN. However, the observed CN is around 4, which corresponds to an actual CN of about 5.3 if we take into account the As(III) fraction as done above ($4 \cdot 4/3 = 5.3$), that is definitively too large for randomly distributed/highly diluted As(III). The observed CN, rescaled by the fraction of As species which we believe substituted in the calcite lattice (i.e., As(III)), is close to the maximum number of As nearest neighbors in a fully As-substituted calcite structure (CN = 6). This finding support the hypothesis of an As(III) clustering in the calcite structure, in accordance with spectroscopic results provided by Romanelli et al. (2008).

The occurrence of a strong signal from As–Ca (at 3.07 and 3.36 Å) and As–As (at 3.93 Å) coordination shells is a strong evidence that As(III) is bound to the calcite lattice. Support to this hypothesis comes from the comparison between the structural information obtained by EXAFS analysis and the DFT simulations performed replacing a carbonate group with an arsenite one. The experimentally observed coordination shells (As–O, As–Ca1 and As–Ca2) are reproduced with an excellent agreement by DFT simulations (if we consider the discussion done above for the As–O distance). In particular, DFT simulations also confirm the splitting of the As–Ca distances, which is a consequence of the displacement of the As atom along the [0 0 0 1] direction out of the oxygen plane (Fig. 6a) (in this way, As reaches a favorable pyramidal configuration, minimizing the steric effects of the lone pair). The value obtained from DFT simulations for the As displacement along the *c*-axis (0.80 Å) is in good agreement with the value measured by Cheng et al. (1999) in arsenite groups adsorbed onto calcite surface. On the other hand, the increment in the value of the *c* lattice parameter reported by DFT simulations (Table 2) is highly overestimated. This is due to the fact that simulations were performed substituting one $HAsO_3^{2-}$ group for one CO_3 in a single calcite cell, resulting in a As concentration much higher than the real one, and therefore, in an unrealistic elongation of the *c* lattice parameter. We do expect that in As-bearing calcites there is a slight, but measurable, effect of elongation of the *c* parameter. In natural calcites, evidence of this effect could be complicated by other lattice effects due to cation impurities (such as Mg, Fe, Mn).

Although $As^{5+}O_4 \Leftrightarrow CO_3$ substitution was claimed to be observed in synthetic calcite samples (Alexandratos et al., 2007), the occurrence of the arsenate anion in the calcite lattice is unlikely, or in any case minor. The slightly larger size of the tetrahedral $As(V)O_4$ groups, with respect to the pyramidal $As(III)O_3$ group, would favor the isomorphic $As(III)O_3 \Leftrightarrow CO_3$ substitution instead to the $As(V)O_3 \Leftrightarrow CO_3$ one. Accordingly, our findings suggest a scenario in which As(III) mainly substitutes C in the CO_3 group, while As(V) is present as an adsorbed oxyanion onto Fe-oxyhydroxides.

It is noteworthy to mention that Alexandratos et al. (2007), who claimed that arsenate group (AsO_4^{3-}) replaces carbonate in calcite, found two distinct As–Ca distances (~3.4 and ~3.6 Å), which are longer than those found in this study. This finding strengthens the idea that we are dealing with a different mechanism of As uptake when compared to Alexandratos et al. (2007).

The hypothesis that As is bound in the calcite lattice is also supported by the conclusion of the ESEEM study by Di Benedetto et al. (2006). The As–Ca distance suggested by these authors, ~3.2 Å, was inferred by the distance between As and Mn substituting for Ca in the calcite lattice, assuming a similar deformation of the calcite lattice in the case of co-uptake by As and Mn. The distance value proposed by Di Benedetto et al. (2006) is in full agreement with the average of the distances observed by EXAFS, 3.07–3.36 Å (notice that modeling of ESEEM data provides only an average of the possible anisotropic location of interacting nuclei in the shells around the paramagnetic center).

The presence of arsenite groups in the calcite structure necessarily implies that there was an interaction between arsenite and the calcite surface during the precipitation of this mineral in the PRV travertine. Sø et al. (2008), in contrast with the experimental results of Roman-Ross et al. (2006), contend that this interaction is negligible unless at pH (~9.5) and As concentrations (>50 μM) that are unlikely to occur in natural environments. We are not able to solve the contradiction between the laboratory data by Roman-Ross et al. (2006) and Sø et al. (2008), although we notice that the first is a co-precipitation experiment and the second an adsorption one. Moreover, in natural environ-

ments additional factors can occur (e.g., mediation by microorganisms, Oremland and Stolz, 2003; Oremland et al., 2005 and reference therein), inducing a different behavior with respect to laboratory conditions. We notice, for example, that point of zero charge of calcite surface occurs at pH values in the range 9–10 (Sadiq, 1997), meaning that the surface of calcite is positively charged at pH values lower than this threshold. It is expected that the OH^- concentration near to the calcite surface is higher than in the bulk solution when the net surface charge of this mineral is positive. In fresh water, the counter-ions (mainly OH^-) layer thickness next to the calcite surface can extend up to ~100 Å in the solution (Appelo and Postma, 2007). Some As reducing bacteria (driving the As(V)–As(III) reaction) are thought to be insensitive to As-rich conditions only in high pH environments, where As(III) species are charged and thus cannot enter the cell (Oremland and Stolz, 2003). In fact, optimal growth conditions for As reducing bacteria are matched at pH ~9.5 in continental lakes (Oremland et al., 2005). The local high-pH environment next to positively charged mineral surface may led to the dissociation of arsenious acid and its migration toward the positive surface causing adsorption and coprecipitation observed, under laboratory conditions, by Roman-Ross et al., 2006. In systems characterized by diffusive ion transport and by high specific surface of the precipitating mineral, such as in a lake where calcite precipitates in micro-crystals, these processes are feasibly maximized. However, it is also well known that precipitation rate can strongly affect the incorporation of trace elements into minerals: for instance, high As(V) levels in garnet were ascribed to rapid precipitation (Charnock et al. 2007). Therefore, in principle, both mechanisms have to be considered concurring in calcite formation. The question remains open to different interpretations and additional studies appear necessary. Nevertheless, we want to stress here that potential important contributions may result from the study of natural systems like the PRV travertine.

It is worth noting that the carbonate replacement by arsenite groups raises a question about charge balance. The simplest way would be uptake of the $HAsO_3^{2-}$ group instead of AsO_3^{3-}, as suggested by Roman-Ross et al. (2006). However, the presence of a protonated oxyanion in this specific sample is contradicted by EPR evidence (Di Benedetto et al., 2006). Two possible alternatives can be considered: a concurrent uptake of a trivalent cation (e.g., Rare Earth Elements) in the octahedral Ca site, or coupled vacancy-replacement processes (i.e., two arsenite groups and a vacancy for three carbonates).

The observed heterogeneity of the samples would beneficiate of the use of micro probe techniques, such Micro-X-Ray Fluorescence (μ-XRF), Micro-X-Ray Diffraction (μ-XRD) and Micro-X-ray Absorption Spectroscopy (μ-XAS), in order to further confirm the results presented in this study. In particular, two dimensional fluorescence elemental mapping with microscopic resolution (μ-XRF), would reveal the association of As with other elements, while μ-XRD and μ-XAS would indicate the crystallographic phases of As and its speciation in selected areas. Proposals for access to high sensitivity microbeam facilities are under consideration.

5. CONCLUSIONS

A characterization of the morphology and composition, oxidation state, short and long range lattice structure of As in natural travertine samples was carried out combining SEM-EDS, X-ray Absorption Spectroscopy (XAS), X-ray Diffraction (XRD), and theoretical *ab initio* simulations.

SEM-EDS revealed a heterogeneous composition of the samples, which is confirmed by structural probe techniques: in two samples, the XANES part of the spectra indicates As(V) in a poorly ordered environment; in the third sample, XANES reveals a coexistence of As(III) and As(V), roughly in a 3:1 ratio. This ratio reflects the relative abundance of As incorporated into calcite and onto Fe/Mn oxyhydroxides.

EXAFS refinements suggest As(III) to occur in a local environment compatible with the structure derived by the substitution of arsenite for carbonate in calcite lattice, as previously suggested by Di Benedetto et al. (2006) on the basis of an EPR-ESE study on same samples. EXAFS data are in excellent agreement with structural DFT simulations performed substituting a CO_3^{2-} unit with a $HAsO_3^{2-}$ group in the calcite cell. EXAFS analysis also suggests the possible clustering of As anionic groups in limited volumes in calcite.

On the contrary, As(V) seems to be present in a poorly crystalline phase, probably adsorbed on Fe-oxyhydroxides.

Recent laboratory studies gave contrasting indications on the interaction of arsenite species with calcite; the results of our study suggest that in natural system this interaction may occur. The fact that only a fraction of the arsenic present in these travertines can be assigned to the carbonate–arsenite substitution, suggests that the process of incorporation of As(III) in calcite can occur, but it is not known whether, in general, this process is effective as the adsorption of As by Fe-oxyhydroxides. We notice that the As hosted in natural calcites is low if there is a competition with iron/manganese oxyhydroxides (see also Le Guern et al., 2003) but the effectiveness of mechanisms controlling the partition of As between these phases is still poorly known. On the other hand, the evidence from laboratory studies that As(III) concentrations in calcite may exceed 2 g/kg (Roman-Ross et al., 2006), suggests that As incorporation by this mineral may become important in conditions (e.g., reducing and/or alkaline environments) where adsorption of As onto iron oxyhydroxides is not favored.

ACKNOWLEDGMENTS

The authors want to express their warmest thanks to Andrea Caneschi and Donella Rovai, University of Florence, and to Luisa Poggi, Museo di Storia Naturale, University of Florence, for providing some standards used in this study. FDB benefited of a research grant funded by the Regional Administration of Tuscany. Authors are indebted with Mario Paolieri and Mauro Rovezzi for their support in the experimental and analytical work. This research was funded by the PRIN 2008 (PC). We also acknowledge

the European Synchrotron Radiation Facility for provision of synchrotron radiation facilities during experiments ME-1182 and EC-130, performed at BM08 (GILDA) beamline.

REFERENCES

Alexandratos V. G., Elzinga E. J. and Reeder R. J. (2007) Arsenate uptake by calcite: macroscopic and spectroscopic characterization of adsorption and incorporation mechanisms. *Geochim. Cosmochim. Acta* **71**, 4172–4187.

Ankudinov A. L., Ravel B., Rehr J. J. and Conradson S. D. (1998) Real-space multiple-scattering calculation and interpretation of X-ray-absorption near-edge structure. *Phys. Rev. B* **58**, 7565–7576.

Appelo C. A. J. and Postma D. (2007) Geochemistry groundwater and pollution. Balkema, p. 649.

Aurelio G., Fernández-Martínez A., Cuello G. J., Roman-Ross G., Alliot I. and Charlet L. (2010) Structural study of selenium(IV) substitutions in calcite. *Chem. Geol.* **270**, 249–256.

Bardelli F., Meneghini C., Mobilio S., Ray S. and Sarma D. D. (2009) Local structure of $Sr_2FeMo_xW_{1-x}O_6$ double perovskites across the composition driven metal to insulator transition. *J. Phys.: Condens. Matter* **21**, 195502.

Becke A. D. (1993) Density functional thermochemistry: the role of exact exchange. *J. Chem. Phys.* **98**, 5648–5652.

Benvenuti M. G., Benvenuti M., Costagliola P. and Tanelli G. (2009) The Quaternary in the mid-upper reach of the Pecora River (southern Tuscany, Italy): implications for the paleohydrographic evolution and surface sediments provenance. *Boll. Soc. Geol. It.* **128**, 61–72.

Broyden C. G. (1970a) The convergence of a class of double-rank minimization Algorithms 1. "General Considerations". *IMA J. Appl. Math.* **6**, 76–90.

Broyden C. G. (1970b) The convergence of a class of double-rank minimization Algorithms 1. "The New Algorithm". *IMA J. Appl. Math.* **6**, 222–231.

Causà M., Dovesi R. and Roetti C. (1991) Pseudopotential Hertree-Fock Study of 17 III-V-Semiconductors. *Phys. Rev. B* **43**, 11937–11943.

Chakraborty S., Bardelli F. and Charlet L. (2010) Reactivities of Fe(II) on calcite: selenium reduction. *Environ. Sci. Technol.* **44**, 1288–1294.

Charnock J. M., Polya D. A., Gault G. and Wogelius R. (2007) Direct EXAFS evidence for incorporation of As^{5+} in the tetrahedral site of natural andraditic garnet. *Am. Mineral.* **92**, 1856–1861.

Cheng L., Fenter P., Sturchio N. C., Zhong Z. and Bedzyk M. J. (1999) X-ray standing wave study of arsenite incorporation at the calcite surface. *Geochim. Cosmochim. Acta* **63**, 3153–3157.

Costagliola P., Benvenuti M., Benvenuti M. G., Innocenti A., Mascaro I., Paolieri M., Rossato L. and Tanelli G. (2004) Arsenic distribution in the Quaternary sediments of the median valley of the Pecora stream (Grosseto, Italy). In *Brownfields II* (eds. A. Donati, C. Rossi and C. A. Brebbia). WIT Press, Southhampton UK, pp. 201–209.

Costagliola P., Rimondi V., Benvenuti M., Chiarantini L., Di Benedetto F., Gasparon M., Lattanzi P. and Paolieri M. (2007) Arsenic uptake by natural calcites: preliminary results from sequential extraction of Travertines (Southern Tuscany, Italy). *IMWA Symposium 2007*: May 27–31 (eds. F. Frau and R. Cidu), Cagliari/Sardinia Italy, pp. 415–418.

Costagliola P., Benvenuti M., Chiarantini L., Bianchi S., Di Benedetto F., Paolieri M. and Rossato L. (2008) Impact of ancient metal smelting on arsenic pollution in the Pecora River Valley, Southern Tuscany, Italy. *Appl. Geochem.* **23**, 1241–1259.

Costagliola P., Benvenuti M. M., Benvenuti M. G., Di Benedetto F. and Lattanzi P. (2010) Quaternary sediment geochemistry as a clue for tracing the source of toxic elements: a case study of arsenic in the Pecora Valley (southern Tuscany, Italy). *Chem. Geol.* **270**, 80–89.

Di Benedetto F., Costagliola P., Benvenuti M., Lattanzi P., Romanelli M. and Tanelli G. (2006) Arsenic incorporation in natural calcite lattice Evidence from electron spin echo spectroscopy. *Earth Planet. Sci. Lett.* **246**, 458–465.

Dixit S. and Hering J. G. (2003) Comparision of arsenic (V) and arsenic (III) sorption on to iron oxide minerals: implication for arsenic mobility. *Environ. Sci. Technol.* **37**, 4182–4189.

Dovesi R., Saunders V. R., Roetti C., Orlando R., Zicovich-Wilson C. M., Pascale F., Civalleri B., Doll K., Harrison N. M., Bush I. J., D'Arco P., Llunell M. (2006) CRYSTAL06 User's Manual, Torino (Italy).

Fenter P. A, Rivers M. L., Sturchio N. C. and Sutton S. R. (2002) Applications of synchrotron radiation in low-temperature geochemistry and environmental science. *Reviews in Mineralogy and Geochemistry*, 49, Mineralogical Society, Washington.

Fernández-Martínez A., Cuello G. J., Jonson M. R., Bardelli F., Román-Ross G., Charlet L. and Turrillas X. (2008) Arsenate incorporation in gypsum probed by neutron, X-ray scattering and density functional theory modeling. *J. Phys. Chem. A* **112**, 5159–5166.

Ferraris G., Jones D. W. and Sowden J. M. (1974) Hydrogen bonding in the crystalline state. A neutron and X-ray diffraction study of $NaH_2AsO_4{\cdot}H_2O$, a crystal structure with unusual pseudo-symmetry. *Atti Accademia Scienze Torino* **108**, 507–527.

Fletcher R. (1970) A new approach to variable metric algorithms. *Comput. J.* **13**, 317–322.

Goldberg S. and Glaubig R. (1988) Anion sorption on a calcareous, montmorillonitic soil–arsenic. *Soil Sci. Soc. Am. J.* **52**, 1297–1300.

Goldfarb D. (1970) A family of variable-metric methods derived by variational means. *Math. Comp.* **24**, 23–26.

Gopal R. and Calvo C. (1971) Crystal structure of $Ca_3(AsO_4)_2$. *Canad. J. Chem.* **49**, 1036–1046.

Isaure M. P., Laboudigue A., Manceau A., Sarret G., Tiffreau C., Trocellier P., Lamble G., Hazemann J. L. and Chateigner L. (2002) Quantitative Zn speciation in a contaminated dredged sediment by mu-PIXE, mu-SXRF, EXAFS spectroscopy and principal component analysis. *Geochim. Cosmochim. Acta* **66**, 1549–1567.

James F. and Winkler M. (2004) Available from: <http://www.cern.ch/minuit>.

Jansen E., Kyek A., Schafer W. and Schwertmann U. (2002) The structure of six-line ferrihydrite. *Appl. Phys. A* **74**, S1004–S1006.

Jansen M. Z. (1979) Ueber eine neue Modifikation von As_2O_5. *Naturforsch. B* **34**, 10–13.

Jia Y., Xu L., Wang X. and Demopoulos G. P. (2007) Infrared spectroscopic and X-ray diffraction characterization of the nature of adsorbed arsenate on ferrihydrite. *Geochim. Cosmochim. Acta* **71**(7), 1643–1654.

Jönsson J. and Sherman D. M. (2008) Sorption of As(III) and As(V) to siderite, green rust (fougerite) and magnetite: implications for arsenic release in anoxic groundwaters. *Chem. Geol.* **255**, 173–181.

Kitahama K., Kiriyama R. and Baba Y. (1975) Refinement of the crystal structure of scorodite. *Acta Crystallogr. B* **31**, 322–324.

Lee C., Yang W. and Parr R. G. (1988) Development of the Colle-Salvetti correlation-energy formula into a functional of the electron density. *Phys. Rev. B* **37**, 785–789.

Lee P. A., Citrin P. H., Eisenbergher P. and Kincaid B. M. (1981) Extended X-ray absorption fine structure – its strengths and limitations as a structural tool. *Rev. Mod. Phys.* **53**, 769–806.

Le Guern C., Baranger P., Crouzet C., Bodénan F. and Conil P. (2003) Arsenic trapping by iron oxyhydroxides and carbonates at hydrothermal spring outlets. *Appl. Geochem.* **18**, 1313–1323.

Lenoble V., Bouras O., Deluchat V., Serpaud B. and Bollinger J. C. (2002) Arsenic adsorption onto pillard clays and iron oxides. *J. Colloid Interface Sci.* **255**, 52–58.

Markgraf S. A. and Reeder R. J. (1985) High-temperature structure refinements of calcite and magnesite. *Am. Mineral.* **70**, 590–600.

Matschullat J. (2000) Arsenic in the geosphere – a review. *Sci. Total Environ.* **249**, 297–312.

Menary J. W. (1958) The crystal structure of sodium polymeta-arsenite ($NaAsO_2$). *Acta Crystallogr.* **11**, 742–743.

Monesi C., Meneghini C., Bardelli F., Benfatto M., Mobilio S., Manju U. and Sarma D. D. (2005) Local structure in $LaMnO_3$ and $CaMnO_3$ perovskites: a quantitative structural refinement of Mn-K edge XANES data. *Phys. Rev. B* **74**, 174104.

Nriagu J. (1994) *Arsenic in the Environment. Part I: Cycling and Characterization*. Wiley Interscience Publication, New York.

Oremland R. S. and Stolz J. F. (2003) The ecology of Arsenic. *Science* **300**, 939–944.

Oremland R. S., Kulp T. R., Blum J. S., Hoeft S. E., Baesman S., Miller L. G. and Stolz J. F. (2005) A microbial arsenic cycle in a salt-saturated, extreme environment. *Science* **308**, 1305–1308.

Ouvrard S., de Donato P., Simonnot M. O., Begin S., Ghanbaja J., Alnot M., Duval Y. B., Lhote S., Barres O. and Sardin M. (2005) Natural manganese oxide: combined analytical approach for solid characterization and arsenic retention. *Geochim. Cosmochim. Acta* **69**, 2715–2724.

Pascarelli S., Boscherini F., D'Acapito F., Hrdy J., Meneghini C. and Mobilio S. (1996) X-ray optics of a dynamical sagittal-focusing monochromator on the GILDA beamline at the ESRF. *J. Synch. Rad.* **3**, 147–155.

Pentecost A. (1995) The quaternary travertine deposits of Europe and Asia Minor. *Quat. Sci. Rev.* **14**, 1005–1028.

Pertlik F. (1978) Structure refinement of cubic As_2O_3 (arsenolite) with single crystal data. *Czech. J. Phys. B* **28**, 170–176.

Ramírez-Solís A., Mukopadhyay R., Rosen B. P. and Stemmler T. L. (2004) Experimental and theoretical characterization of arsenite in water: insights into the coordination environment of As–O. *Inorg. Chem.* **43**(9), 2954–2959.

Ravel B. (2001) ATOMS: crystallography for the X-ray absorption spectroscopist. *J. Synch. Rad.* **8**, 314–316.

Rehr J. J. and Albers R. C. (2000) Theoretical approaches to X-ray absorption fine structure. *Rev. Mod. Phys.* **72**, 621–654.

Roman Ross G., Cuello G. J., Turrillas X., Fernandez Martinez A. and Charlet L. (2006) Arsenite sorption and co-precipitation with calcite. *Chem. Geol.* **233**, 328–336.

Romanelli M., Benvenuti M., Costagliola P., Di Benedetto F., Lattanzi P. (2008) Electron Spin Echo invesitgation of Mn(II)-As interaction in calcite, $CaCO_3$: towards a quantitative model. *Atti del 1 Meeting SIMP-AIC*, Sestri Levante, 7–12 settembre 2008.

Saalfield S. L. and Bostick B. C. (2009) Changes in iron, sulfur, and arsenic speciation associated with bacterial sulfate reduction in ferrihydrite-rich systems. *Environ. Sci. Technol.* **43**, 8787–8793.

Sadiq M. (1997) Arsenic chemistry in soils: an overview of thermodynamic predictions and field observations. *Water, Air Soil Contam.* **93**, 117–136.

Shanno D. (1970) Conditioning of quasi-Newton methods for function minimization. *Math. Comp.* **24**, 647–656.

Sherman D. M. and Randall S. R. (2003) Surface complexation of arsenic (V) to iron(III) hydroxides: structural mechanism from ab initio molecular geometries and EXAFS spectroscopy. *Geochim. Cosmochim. Acta* **67**, 4223–4230.

Schwertmann U., Staniek H. and Becher H.-H. (2004) Long-term in vitro transformation of 2-line ferrihydrite to goethite/hematite at 4, 10, 15 and 25 °C. *Clay Mineral* **39**(4), 433–438.

Smedley P. L. and Kinninburg D. G. (2002) A review of the source, behaviour and distribution of arsenic in natural waters. *Appl. Geochem.* **17**, 517–568.

Sø H. U., Postma D., Jakobsen R. and Larsen F. (2008) Sorption and desorption of arsenate and arsenite on calcite. *Geochim. Cosmochim. Acta* **72**, 5871–5884.

Tang Y., Elzinga E. J., Lee Y. J. and Reeder R. J. (2007) Coprecipitation of chromate with calcite: batch experiments and X-ray absorption spectroscopy. *Geochim. Cosmochim. Acta* **71**, 1480–1493.

Tufano K. J., Reyes C., Saltikov C. and Fendorf S. (2008) Reductive processes controlling arsenic retention: revealing the relative importance of iron and arsenic reduction. *Environ. Sci. Technol.* **42**, 8283–8289.

Valenzano L., Torres F. J., Doll K., Pascale F., Zicovich-Wilson C. M. and Dovesi R. Z. (2006) Ab initio study of the vibrational spectrum and related properties of crystalline compounds; the case of $CaCO_3$ calcite. *Z. Phys. Chem.* **220**, 893–912.

Yokoyama Y., Mitsunobu S., Tanaka K., Itai T. and Takahashi Y. (2009) A study on the coprecipitation of arsenite and arsenate into calcite coupled with the determination of oxidation states of arsenic both in calcite and water. *Chem. Lett.* **38**, 910–911.

Wilke M., Farges F., Petit P. E., Brown, Jr., G. E. and Martin F. (2001) Oxidation state and coordination of Fe in minerals: an Fe K-XANES spectroscopic study. *Am. Miner.* **86**, 714–730.

Associate editor: Roy A. Wogelius